SCIENCE CHINA
Information Sciences

• RESEARCH PAPER •

September 2020, Vol. 63 192205:1–192205:13
https://doi.org/10.1007/s11432-019-2639-6

Learning impedance control of robots with enhanced transient and steady-state control performances

Tairen SUN[1], Long CHENG[1], Liang PENG[1], Zengguang HOU[1*] & Yongping PAN[2]

[1]*State Key Laboratory of Management and Control for Complex Systems, Institute of Automation, Chinese Academy of Sciences, Beijing* 100190*, China;*
[2]*School of Data and Computer Science, Sun Yat-sen University, Guangzhou* 510006*, China*

Received 30 March 2019/Accepted 5 August 2019/Published online 24 July 2020

Abstract This study proposes a learning impedance controller comprising a proportional feedback control term, a composite-learning-based uncertainty estimation term, and a robot-environment interaction control term. The impedance control problem is converted into a particular reference-trajectory tracking problem based on a generated reference trajectory. The proposed controller ensures the exponential convergence of the auxiliary tracking error and the uncertainty estimation error. The interaction control term improves the transient control performance through suppression/encouragement of the incorrect/correct robot movements. The composite-learning update law enhances the transient and steady-state control performances based on the exponential convergence of the uncertainty estimation error and auxiliary tracking error. Finally, the effectiveness and advantages of the proposed impedance controller are validated by theoretical analysis and simulations on a parallel robot.

Keywords robot, adaptive control, neural network, impedance control, parameter convergence

Citation Sun T R, Cheng L, Peng L, et al. Learning impedance control of robots with enhanced transient and steady-state control performances. Sci China Inf Sci, 2020, 63(9): 192205, https://doi.org/10.1007/s11432-019-2639-6

1 Introduction

Compliant robot behaviour is required when a robot comes in contact with its environment. However, such behavior cannot be ensured using position control strategies [1–4]. Impedance control of robots, originally proposed by Hogan in the late 1980s, is one of the most powerful compliance control methods [5–8] and has been applied in robot-assisted rehabilitation [9, 10], robot-assisted walking [11], robot-assisted assembly, and human-robot collaboration [12].

An impedance controller aims to obtain the desired spring-damping dynamics between the desired-trajectory tracking error and the robot-environment interaction force. Over the past decades, numerous impedance control laws have been designed for robots in case of robot-environment interaction [13]. However, some existing impedance controllers fail to guarantee the convergence of impedance errors to zero or its small neighborhoods [14–18]. This failure has been observed to affect the stability and reliability of the impedance controllers [14–18]. Uncertainties and disturbances in robot modeling are among the most important factors that affect impedance control performances. Thus, designing robust impedance controllers to improve impedance control performances continues to be a significant research topic.

Sliding-mode impedance control is one possible approach for improving the impedance control performance [19,20]. In spirit of robust passivity-based control, the desired impedance dynamics can be achieved

* Corresponding author (email: zengguang.hou@ia.ac.cn)

by reaching a sliding surface constructed by the switching function and its time derivative [19,20]. In [19], a sliding-mode impedance controller was proposed with the switching function reaching zero in finite time. After this finite time, the switching function remains constant at zero, and the desired sliding surface can be theoretically achieved. However, chattering severely affects the impedance control performance and achievement of the desired impedance dynamics. In [20], a dead-zone strategy was applied to alleviate chattering problem in a sliding-mode impedance controller. However, this strategy may not effectively decrease chattering and may lead to difficulties in arriving at the desired sliding surface, which will affect the impedance control performances.

In the previous few decades, iterative-learning-based and adaptive impedance controllers have been proposed for improving the impedance control performance under the assumption that the desired impedance dynamics can be factorized in real number field [21–25]. However, these impedance controllers suffer from following deficiencies: (1) The assumption of factorizability with respect to the desired impedance dynamics in real number field severely limits the controller applications. (2) Iterative learning controllers may be fit only for robots in repeated actions, limiting the applications of the iterative learning impedance controllers [21–23]. (3) The adaptive impedance controllers proposed in previous studies [24,25] can be used to obtain the boundedness of impedance errors; however, they cannot ensure good transient impedance control performance and cannot achieve convergence of impedance errors to zero. The recently proposed composite learning impedance controller (CLIC) [26] has ensured the convergence of the impedance error to zero and improved the impedance control performance; however, the factorizability of the desired impedance dynamics in real number field is still required. Based on a constructed impedance trajectory, an adaptive fuzzy neural impedance controller was designed for robots in a previous study [27] without the factorizability assumption; however, this controller still suffers from the third deficiency mentioned above.

In almost all the impedance controllers [13–27], robot-environment interaction forces are completely compensated; this compensation leads to control conservativeness. Further, interaction forces can be used to enhance the transient impedance control performance. If the robot-environment interaction forces can boost the convergence of impedance errors, robot movements can be considered as correct and should be encouraged. Otherwise, the robot movements will be considered incorrect and requiring suppression. A previous study [28] proposed multi-model control for robotic exoskeletons driven by series elastic actuators. The proposal used an interaction control term to improve the transient control performance by rejecting/encouraging incorrect/correct movements. However, the implementation of the interaction control term requires estimation of the high-order derivatives of joint positions, which introduces difficulties in terms of control implementation.

Based on the generated reference trajectory, we propose a CLIC comprising a proportional feedback control term, a composite-learning-based uncertainty estimation term, and an interaction control term. When compared with the existing impedance controllers, the contributions and innovation of this study can be given as follows:

(1) The proposed CLIC enhances the transient and steady-state impedance control performances through exponential convergence of the generated-reference trajectory tracking error and the uncertainty estimation error.

(2) The robot-environment interaction control term improves the transient impedance control performance through suppression/encouragement of incorrect/correct robot movements without estimating the high-order derivatives of angle positions.

(3) The factorizability of the desired impedance dynamics in real number field is not required in the impedance control design.

2 Problem formulation

Consider a robot with the following Euler-Lagrangian dynamics:

$$M(q)\ddot{q} + C(q,\dot{q})\dot{q} + G(q) + F(\dot{q}) = u + \tau_e, \tag{1}$$

where $q \in \mathbb{R}^n$, $\dot{q} \in \mathbb{R}^n$ and $\ddot{q} \in \mathbb{R}^n$ denote the joint angular position, the joint angular velocity, and the joint angular acceleration, respectively; $M(q) \in \mathbb{R}^{n\times n}$ denotes the inertia matrix of the rigid body; $C(q,\dot{q}) \in \mathbb{R}^{n\times n}$ denotes the Coriolis and centripetal matrix; $G(q) \in \mathbb{R}^n$ denotes the gravitational torque; $F(\dot{q}) \in \mathbb{R}^n$ denotes the friction force; $u(t) \in \mathbb{R}^n$ is the control input; and $\tau_e \in \mathbb{R}^n$ denotes the interaction force in the joint space.

The robot dynamics described by (1) exhibits the following properties.

Property 1. $M(q)$ is a positive definite matrix; i.e., there exist positive constants σ_1 and σ_2, such that $\sigma_1 I \leqslant M(q) \leqslant \sigma_2 I$ with I being the $n \times n$-sized identity matrix.

Property 2. The system uncertainties can be linearly expressed as

$$M(q)\phi_1 + C(q,\dot{q})\phi_2 + G(q) + F(\dot{q}) = Y(\phi_1,\phi_2,q,\dot{q})\theta, \tag{2}$$

where ϕ_1 and ϕ_2 are the auxiliary vectors, $Y(\phi_1,\phi_2,q,\dot{q}) \in \mathbb{R}^{n\times n_q}$ is a known regression matrix, and $\theta \in \mathbb{R}^{n_q}$ is an unknown constant vector.

Property 3. The matrix $\dot{M}(q) - 2C(q,\dot{q})$ is skew-symmetric.

Further, we present the following robot dynamics assumption and definitions of persistent excitation (PE) and interval excitation (IE) to facilitate impedance control design.

Assumption 1. The desired trajectory q_d and its time derivatives $\dot{q}_d$ and $\ddot{q}_d$ are bounded.

Definition 1. A bounded signal $W(t) \in \mathbb{R}^{n\times n_q}$ is of IE over $t \in [T_e - \tau_d, T_e]$ with $\tau_d > 0$ and $T_e > \tau_d$ if and only if there exists $\rho > 0$ such that $\int_{T_e-\tau_d}^{T_e} W(\sigma)^{\mathrm{T}} W(\sigma)\mathrm{d}\sigma \geqslant \rho I$.

Definition 2 ([29])**.** A bounded signal $W(t) \in \mathbb{R}^{n\times n_q}$ is of PE if and only if there exist $\rho > 0$ and $\tau_d > 0$ such that $\int_{t-\tau_d}^{t} W(\sigma)^{\mathrm{T}} W(\sigma)\mathrm{d}\sigma > \rho I$ for all $t > 0$.

The study aims to design a composite learning controller to obtain the following spring-damping dynamics:

$$-\tau_e = M_d(\ddot{q}_d - \ddot{q}) + B_d(\dot{q}_d - \dot{q}) + K_d(q_d - q), \tag{3}$$

which is equivalent to

$$\ddot{q} + M_d^{-1}B_d\dot{q} + M_d^{-1}K_d q = \ddot{q}_d + M_d^{-1}B_d\dot{q}_d + M_d^{-1}K_d q_d + M_d^{-1}\tau_e, \tag{4}$$

where M_d, B_d, and K_d are the desired inertia matrix, the desired damping matrix, and the desired stiffness matrix, respectively, which are diagonal and positive definite.

3 Impedance control design

Define the impedance error e as

$$e = M_d(\ddot{q}_d - \ddot{q}) + B_d(\dot{q}_d - \dot{q}) + K_d(q_d - q) + \tau_e. \tag{5}$$

It is obvious that the desired impedance dynamics in (3) can be accurately achieved if and only if the impedance error e converges to zero as $t \to \infty$.

Let the reference trajectory q_r for the robot be generated by

$$(s^2 I + M_d^{-1}B_d s + M_d^{-1}K_d)q_r = \ddot{q}_d + M_d^{-1}B_d\dot{q}_d + M_d^{-1}K_d q_d + M_d^{-1}\tau_e, \tag{6}$$

where s is a differential operator. Based on (4)–(6), the impedance error e can be presented as

$$e = M_d(\ddot{q}_r - \ddot{q}) + B_d(\dot{q}_r - \dot{q}) + K_d(q_r - q) = M_d\ddot{e}_1 + B_d\dot{e}_1 + K_d e_1, \tag{7}$$

where $e_1 = q_r - q$ is the reference-trajectory tracking error.

If $e_1 \to 0$, $\dot{e}_1 \to 0$, and $\ddot{e}_1 \to 0$ as $t \to \infty$, then, from (7), we can observe that the impedance error e converges to zero as $t \to \infty$, and the desired impedance dynamics can be achieved. In the following of this section, we design a CLIC, such that $e_1 \to 0$, $\dot{e}_1 \to 0$, and $\ddot{e}_1 \to 0$ can be given as $t \to \infty$.

Remark 1. If the impedance error e converges to zero or its small neighborhoods, impedance control stability can be obtained and the desired impedance dynamics can be achieved accurately or with a small error. Otherwise, the desired impedance dynamics cannot be obtained.

Remark 2. The convergence of a signal to zero cannot ensure the convergence of the time derivative of the signal to zero. For example, the function $10e^{-t}\sin(e^t)$ converges to zero as $t \to +\infty$; but its time derivative $-10e^{-t}\sin(e^t) + 10\cos(e^t)$ will not converge to zero as $t \to +\infty$. Thus, the convergence of e_1 alone or even of both $e_1, \dot{e}_1$ cannot ensure the convergence of $\ddot{e}_1$ and the convergence of the impedance error e.

Remark 3. The dynamics in (6) can be expressed as

$$\begin{bmatrix} \dot{q}_r \\ \ddot{q}_r \end{bmatrix} = A \begin{bmatrix} q_r \\ \dot{q}_r \end{bmatrix} + \begin{bmatrix} 0 \\ \xi \end{bmatrix}, \tag{8}$$

with $\xi = \ddot{q}_d + M_d^{-1}B_d\dot{q}_d + M_d^{-1}K_d q_d + M_d^{-1}\tau_e$ and

$$A = \begin{bmatrix} 0 & I \\ -M_d^{-1}K_d & -M_d^{-1}B_d \end{bmatrix}. \tag{9}$$

Because M_d, B_d, and K_d are diagonal and positive definite matrices, matrix A is Hurwitz. Based on the boundedness of τ_e, q_d, $\dot{q}_d$, and $\ddot{q}_d$, we can conclude that q_r, $\dot{q}_r$, and $\ddot{q}_r$ are bounded and that the generated reference q_r is reasonable.

Remark 4. In traditional robot tracking problems [1–4], only the convergence of the tracking error e_1 has to be obtained. Based on the generated reference trajectory q_r, the impedance control problem is converted into a particular tracking problem, whose particularity lies in requiring the achievement of convergence of not only e_1 but also $\dot{e}_1$ and $\ddot{e}_1$. It quickly becomes clear that the reference-trajectory tracking problem is considerably difficult than the traditional tracking problem.

Define the error e_2 as

$$e_2 = \dot{e}_1 + k_1 e_1. \tag{10}$$

If e_2 and $\dot{e}_2$ converge to zero as $t \to \infty$, then $e_1 \to 0$, $\dot{e}_1 \to 0$, and $\ddot{e}_1 \to 0$ as $t \to \infty$; therefore the impedance error e will converge to zero. Based on (1) and (10), we obtain

$$\begin{aligned} M(q)\dot{e}_2 =& -C(q,\dot{q})e_2 + M(q)(\ddot{q}_d + k_1\dot{e}_1) + C(q,\dot{q})(\dot{q} + e_2) + G(q) + F(q) - u - \tau_e \\ =& -C(q,\dot{q})e_2 + Y(\ddot{q}_d + k_1\dot{e}_1, \dot{q} + e_2, q, \dot{q})\theta - u - \tau_e. \end{aligned} \tag{11}$$

It is convenient to design the impedance controller u as

$$\begin{aligned} u =& -k_2 e_2 - \beta(e_2, \tau_e) + \hat{M}(\ddot{q}_d + k_1\dot{e}_1) + \hat{C}(\dot{q} + e_2) + \hat{G} + \hat{F} \\ =& k_2 e_2 + Y(\ddot{q}_d + k_1\dot{e}_1, \dot{q} + e_2, q, \dot{q})\hat{\theta} - \beta(e_2, \tau_e), \end{aligned} \tag{12}$$

where k_2 is the positive control gain; $\hat{M}, \hat{C}, \hat{G}$, and $\hat{F}$ are the estimators of $M(q)$, $C(q,\dot{q})$, $G(q)$, and $F(\dot{q})$, respectively; $\hat{\theta}$ is the estimator of θ; and $\beta(r, \tau_e)$ is designed to suppress/encourage incorrect/correct robot movements and can be defined as

$$\beta(e_2, \tau_e) = \begin{cases} \left[1 + \tanh\left(\dfrac{e_2^{\mathrm{T}}\tau_e}{-\epsilon}\right)\right]\tau_e, & \text{if } -e_2^{\mathrm{T}}\tau_e \leqslant 0, \\ \tau_e, & \text{else}, \end{cases} \tag{13}$$

with ϵ being a small positive constant.

Substituting (12) into (11) yields

$$M(q)\dot{e}_2 = -C(q,\dot{q})e_2 - k_2 e_2 + \beta(e_2, \tau_e) - \tau_e + Y(\ddot{q}_d + k_1\dot{e}_1, \dot{q} + e_2, q, \dot{q})\tilde{\theta}, \tag{14}$$

where $\tilde{\theta} = \theta - \hat{\theta}$ is the parameter estimation error.

Remark 5. If $-e_2^{\mathrm{T}}\tau_e > 0$, the interaction force can decrease the convergence of e_2, where the robot movement is considered as incorrect. In such cases, $\beta(e_2, \tau_e) = \tau_e$ will be used to suppress the incorrect movement. If $-e_2^{\mathrm{T}}\tau_e \leqslant -\epsilon$, the interaction force can boost the convergence of e_2, where the robot movement is considered as correct. In such cases, $\beta(e_2, \tau_e) = 0$ will be used to encourage the movement. The zone $-\epsilon < -e_2^{\mathrm{T}}\tau_e < 0$ is treated as a transition stage to ensure the continuity of $\beta(e_2, \tau_e)$.

The composite learning law is updated by error e_2 and a model prediction error. To construct the prediction error, we pass the dynamics described by (1) through the following low-pass filter:

$$\Phi(s) = \frac{\alpha}{s+\alpha}, \tag{15}$$

with $\phi(t) = \alpha e^{-\alpha t}$ being the impulse response of $\Phi(s)$. Further, convolving both sides of (1) by $\phi(t)$ yields

$$\phi(t) * Y(\ddot{q}, \dot{q}, q, \dot{q})\theta = \phi(t) * (u(t) + \tau_e(t)) \triangleq y(t). \tag{16}$$

Define $W(q, \dot{q})$ as

$$W(q, \dot{q}) = \phi(t) * Y(\ddot{q}, \dot{q}, q, \dot{q}). \tag{17}$$

Then, from (16) and (17), we obtain

$$W(q, \dot{q})\theta = y(t). \tag{18}$$

Assume $W(q, \dot{q})$ is of IE over $t \in [T_e - \tau_d, T_e]$ as in Definition 1. Define the prediction error as $e_p = Q_e\tilde{\theta}$, where

$$Q_e = \begin{cases} 0, & \text{for } t < T_e, \\ Q(T_e), & \text{for } t \geqslant T_e, \end{cases} \tag{19}$$

and

$$Q(t) = \int_{t-\tau_d}^{t} W(q(\tau), \dot{q}(\tau))^{\mathrm{T}} W(q(\tau), \dot{q}(\tau))\mathrm{d}\tau. \tag{20}$$

Subsequently, the composite learning update law of $\hat{\theta}$ can be obtained as

$$\dot{\hat{\theta}} = \gamma(Y^{\mathrm{T}}(\ddot{q}_d + k_1\dot{e}_1, \dot{q} + e_2, q, \dot{q})e_2 + k_p e_p), \tag{21}$$

where γ denotes a positive learning rate and k_p denotes a positive weight factor.

Theorem 1. Consider a robot with the dynamics described using (1) and that Assumption 1 is satisfied. Let us design a CLIC as in (12) using the composite learning law presented in (21). Further, under the IE condition, the errors e_2 and $\tilde{\theta}$ will converge to zero as $t \to \infty$, and the desired impedance dynamics can be achieved.

Proof. Consider the following Lyapunov function candidate:

$$V = \frac{1}{2}e_2^{\mathrm{T}} M(q) e_2 + \frac{1}{2\gamma}\tilde{\theta}^{\mathrm{T}}\tilde{\theta}. \tag{22}$$

Taking the time derivative of V and substituting (14) into $\dot{V}$, we obtain

$$\begin{aligned} \dot{V} &= e_2^{\mathrm{T}} M(q)\dot{e}_2 + \frac{1}{2}e_2^{\mathrm{T}}\dot{M}(q)e_2 - \frac{1}{\gamma}\tilde{\theta}^{\mathrm{T}}\dot{\hat{\theta}} \\ &= -k_2 e_2^{\mathrm{T}} e_2 + \frac{1}{2}e_2^{\mathrm{T}}(\dot{M}(q) - 2C(q, \dot{q}))e_2 - \tilde{\theta}^{\mathrm{T}}(\dot{\hat{\theta}}/\gamma - Y^{\mathrm{T}}(\ddot{q}_d + k_1\dot{e}_1, \dot{q} + e_2, q, \dot{q})e_2) + e_2^{\mathrm{T}}(\beta(e_2, \tau_e) - \tau_e). \end{aligned} \tag{23}$$

Because the matrix $\dot{M}(q)-2C(q,\dot{q})$ is skew symmetric, $e_2^{\mathrm{T}}(\dot{M}(q)-2C(q,\dot{q}))e_2=0$. Based on the definition of $\beta(e_2,\tau_e)$ in (13), we obtain

$$e_2^{\mathrm{T}}(\beta(e_2,\tau_e)-\tau_e)=\begin{cases}0, & \text{if } -e_2^{\mathrm{T}}\tau_e>0,\\ -e_2^{\mathrm{T}}\tau_e, & \text{if } -e_2^{\mathrm{T}}\tau_e<-\epsilon,\\ \tanh\left(\dfrac{e_2^{\mathrm{T}}\tau_e}{-\epsilon}\right)e_2^{\mathrm{T}}\tau_e, & \text{else.}\end{cases}\tag{24}$$

Thus, $e_2^{\mathrm{T}}(\beta(e_2,\tau_e)-\tau_e)\leqslant 0$. Then, using (23) and (24), we can obtain

$$\dot{V}\leqslant-\tilde{\theta}^{\mathrm{T}}(\dot{\hat{\theta}}/\gamma-Y^{\mathrm{T}}(\ddot{q}_d+k_1\dot{e}_1,\dot{q}+e_2,q,\dot{q})e_2)-k_2e_2^{\mathrm{T}}e_2.\tag{25}$$

Substituting the composite learning law in (21) into (25) yields

$$\begin{aligned}\dot{V}&\leqslant-k_2e_2^{\mathrm{T}}e_2-k_p\tilde{\theta}^{\mathrm{T}}e_p\\&\leqslant-k_2e_2^{\mathrm{T}}e_2-k_p\tilde{\theta}^{\mathrm{T}}Q_e\tilde{\theta}.\end{aligned}\tag{26}$$

Based on the definition of Q_e, we can observe that for $t>0$,

$$\dot{V}(t)\leqslant-k_2e_2^{\mathrm{T}}e_2.\tag{27}$$

Thus, $V(t)$, $\tilde{\theta}$, and e_2 are bounded for $t>0$. From the boundedness of q_r, $\dot{q}_r$, q_d, $\dot{q}_d$, and $\ddot{q}_d$, we can observe that q, $\dot{q}$, and the right side of (14) are bounded. Thus, e_2 is consistently continuous on $t\in[0,\infty)$. By integrating both sides of (27) from $t=0$ to ∞, we obtain

$$\int_0^\infty e_2^{\mathrm{T}}e_2\mathrm{d}t\leqslant\frac{1}{k_2}[V(0)-V(\infty)]\leqslant\infty.\tag{28}$$

According to Babalat's lemma, we can conclude that e_2 converges to zero as $t\to\infty$.

For $t\geqslant T_e$,

$$\begin{aligned}\dot{V}&\leqslant-k_2e_2^{\mathrm{T}}e_2-k_p\tilde{\theta}^{\mathrm{T}}Q(T_e)\tilde{\theta}\\&\leqslant-k_2e_2^{\mathrm{T}}e_2-k_p\rho\tilde{\theta}^{\mathrm{T}}\tilde{\theta}\\&\leqslant-\alpha_1V,\end{aligned}\tag{29}$$

where $\alpha_1=\min\{2k_2/\sigma_2,2k_p\rho\gamma\}$, implying that V exponentially converges to zero if $t\geqslant T_e$. Further, e_2 and $\tilde{\theta}$ will converge to zero as $t\to\infty$.

From the convergence of e_2 and the definition $\beta(e_2,\tau_e)$ in (13), we obtain

$$\lim_{t\to\infty}[\beta(e_2,\tau_e)-\tau_e]=0.\tag{30}$$

Then, based on (13) and the convergence of e_2, $\tilde{\theta}$, and $\beta(e_2,\tau_e)-\tau_e$, we can observe that $\dot{e}_2$ converges to zero as $t\to\infty$. From the definitions of e_1 and e_2 and $\dot{e}_2=\ddot{e}_1+k_1\dot{e}_1$, we can conclude that $q\to q_r$, $\dot{q}\to\dot{q}_r$, and $\ddot{q}\to\ddot{q}_r$ as $t\to\infty$ and that the desired impedance dynamics in (3) can be obtained.

Remark 6. By multiplying both the sides of (18) with $W(\theta,\dot{\theta})^{\mathrm{T}}$ and integrating from $t-\tau_d$ to t, we obtian

$$Q(t)\theta=\int_{t-\tau_d}^{t}W(q(\sigma),\dot{q}(\sigma))^{\mathrm{T}}y(\sigma)\mathrm{d}\sigma.\tag{31}$$

Then, $Q_e\theta$ can be calculated, and the update law in (21) can be implemented.

Remark 7. When compared with the existing impedance controllers, the proposed learning impedance controller improves the control stability and robustness through the convergence of the impedance error e and ensures the suppression/encouragement of incorrect/correct robot movements. In the proposed controller, the required IE condition for $W(q,\dot{q})$ is much more easily to be satisfied than the PE condition,

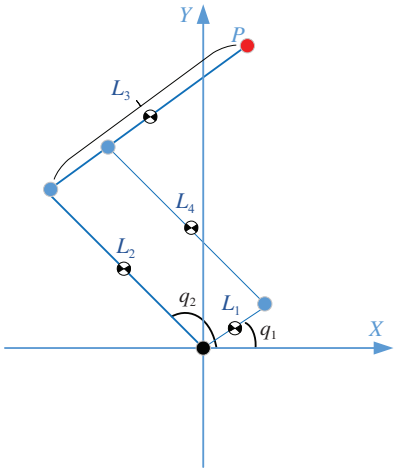

Figure 1 (Color online) Five-bar parallel structure of the considered robot.

which can be easily observed from the definitions of IE and PE and is illustrated in previous studies [29,30]. In the worst case, if the IE condition is never satisfied, then the proposed controller is reduced to a composite adaptive impedance controller, which is also better than the conventional adaptive impedance controllers because of the advantages of better identification effect and smaller tracking error associated with composite adaptive control.

4 Simulation results

The considered robot operates on a five-bar parallel structure (see Figure 1), where link 2 is parallel to link 4 and link 1 is parallel to link 3; further, there is a fifth link at the interaction point P. In the parallel robot, only links 1 and 2 are actuated by the direct current (DC) motors, whereas the others are passive. Thus, there are two degrees of freedom in the robot, identified as angles q_1 and q_2 in Figure 1. The readers can refer to [31] for detailed description of the considered robot. The parallel mechanism exhibits several advantages, such as simple joint design, high stiffness, and low inertia, when compared with its serial counterparts.

The matrices and vectors of the Lagrangian model of the robot can be described as follows [31,32]:

$$M(q)=\begin{bmatrix} M_{11}(q) & M_{12}(q) \\ M_{21}(q) & M_{22}(q) \end{bmatrix},\quad G(q)=[0,0]^{\mathrm{T}},\quad C(q,\dot{q})=\begin{bmatrix} 0 & h\dot{q}_2 \\ -h\dot{q}_1 & 0 \end{bmatrix},$$
$$F(\dot{q})=\mathrm{diag}(k_{v1},k_{v2})\dot{q},\quad \tau_e=J^{\mathrm{T}}(q)f_e, \tag{32}$$

where

$$M_{11}(q)=m_1l_{c1}^2+m_3l_{c3}^2+m_4l_1^2+I_1+I_3,\quad M_{12}(q)=M_{21}(q)=(m_3l_2l_{c3}+m_4l_{c4}^2)\cos(q_2-q_1),$$
$$M_{22}(q)=m_2l_{c2}^2+m_3l_2^2+m_4l_{c4}^2+I_2+I_4,\quad h=-(m_3l_2l_{c3}+m_4l_{c4}^2)\sin(q_2-q_1). \tag{33}$$

Here, l_1, l_2, l_3, and l_4 are the lengths of the joints links L_1, L_2, L_3 and L_4, respectively; l_{c1}, l_{c2}, l_{c3}, and l_{c4} are the distances between the joints and respective centers of mass; I_1, I_2, I_3, and I_4 are the inertial moments of the links; m_1, m_2, m_3, and m_4 are the masses of the links; $J(q)$ is the Jacobian matrix; and f_e is the interaction force at the end effector.

The elements of the regression matrix $Y(\phi_1,\phi_2,q,\dot{q})$ and θ can be described as follows:

$$Y_{11}=\phi_{11},\ Y_{12}=\phi_{12}\cos(q_2-q_1)+\dot{q}_2\phi_{22}\sin(q_1-q_2),\ Y_{13}=Y_{15}=0,\ Y_{14}=\dot{q}_1,$$
$$Y_{22}=\phi_{11}\cos(q_2-q_1)+\dot{q}_1\phi_{21}\sin(q_2-q_1),\ Y_{23}=\phi_{12},\quad Y_{25}=\dot{q}_2,\quad Y_{21}=Y_{24}=0,$$
$$\theta_1=m_1l_{c1}^2+m_3l_{c3}^2+m_4l_1^2+I_1+I_3,\ \theta_2=m_3l_2l_{c3}+m_4l_{c4}^2,$$

$$\theta_3 = m_2 l_{c2}^2 + m_3 l_2^2 + m_4 l_{c4}^2 + I_2 + I_4,\ \theta_4 = k_{v1},\ \theta_5 = k_{v2}. \tag{34}$$

In the simulation, the robot parameters are selected as $l_1 = 0.3$ m, $l_2 = l_4 = 0.6$ m, $l_3 = 0.75$ m, $l_{c1} = 0.15$ m, $l_{c2} = l_{c4} = 0.3$ m, $l_{c3} = 0.375$ m, $I_1 = 0.15\,\mathrm{kg}\cdot\mathrm{m}^2$, $I_2 = I_4 = 0.3\,\mathrm{kg}\cdot\mathrm{m}^2$, $I_3 = 0.45\,\mathrm{kg}\cdot\mathrm{m}^2$, $m_1 = 0.75$ kg, $m_2 = m_4 = 1.5$ kg, $m_3 = 2.25$ kg, $k_{v1} = 0.6\,\mathrm{N}\cdot\mathrm{m}\cdot\mathrm{s}$, $k_{v2} = 0.6\,\mathrm{N}\cdot\mathrm{m}\cdot\mathrm{s}$. Then, $\theta_1 = 1.0683, \theta_2 = 0.6413, \theta_3 = 1.68, \theta_4 = \theta_5 = 0.6$. Then, the following results hold:

$$\begin{aligned}
&\phi(t) * \ddot{q}_1 = \dot{\phi}(t) * \dot{q}_1, \quad \phi(t) * \ddot{q}_2 = \dot{\phi}(t) * \dot{q}_2,\\
&\phi(t) * [\ddot{q}_2 \cos(q_2 - q_1) + \dot{q}_2^2 \sin(q_1 - q_2)] = \phi(t) * \left[\frac{\mathrm{d}}{\mathrm{d}t}(\dot{q}_2 \cos(q_2 - q_1)) - \dot{q}_1 \dot{q}_2 \sin(q_2 - q_1)\right]\\
&\qquad = \dot{\phi}(t) * (\dot{q}_2 \cos(q_2 - q_1)) - \phi(t) * [\dot{q}_1 \dot{q}_2 \sin(q_2 - q_1)],\\
&\phi(t) * [\ddot{q}_1 \cos(q_2 - q_1) + \dot{q}_1^2 \sin(q_2 - q_1)] = \phi(t) * \left[\frac{\mathrm{d}}{\mathrm{d}t}(\dot{q}_1 \cos(q_2 - q_1)) + \dot{q}_1 \dot{q}_2 \sin(q_2 - q_1)\right]\\
&\qquad = \dot{\phi}(t) * (\dot{q}_1 \cos(q_2 - q_1)) + \phi(t) * [\dot{q}_1 \dot{q}_2 \sin(q_2 - q_1)].
\end{aligned} \tag{35}$$

Therefore, by convolving each element of the matrix $Y(\ddot{q}, \dot{q}, q, \dot{q})$ with $\phi(t) = \alpha e^{-\alpha t}$, one can obtain the filtered counterpart $W(q, \dot{q})$ as follows:

$$W(q, \dot{q}) = \begin{bmatrix} \dfrac{\alpha s}{s+\alpha}\dot{q}_1 & \dfrac{\alpha s}{s+\alpha}[\dot{q}_2 \cos(q_2 - q_1)] - \dfrac{\alpha}{s+\alpha}[\dot{q}_1 \dot{q}_2 \sin(q_2 - q_1)] & 0 & \dfrac{\alpha}{s+\alpha}\dot{q}_1 & 0 \\ 0 & \dfrac{\alpha s}{s+\alpha}[\dot{q}_1 \cos(q_2 - q_1)] + \dfrac{\alpha}{s+\alpha}[\dot{q}_1 \dot{q}_2 \sin(q_2 - q_1)] & \dfrac{\alpha s}{s+\alpha}\dot{q}_2 & 0 & \dfrac{\alpha}{s+\alpha}\dot{q}_2 \end{bmatrix}. \tag{36}$$

In the control implementation, the initial position and velocity of the manipulator are $q(0) = [0, 0]^{\mathrm{T}}$ rad and $\dot{q}(0) = [0, 0]^{\mathrm{T}}$ rad/s, respectively; τ_d in the IE is selected as $\tau_d = 4$ s, $\alpha = 1$. In the desired impedance model, the desired trajectory $q_d = [q_{d1}, q_{d2}]^{\mathrm{T}}$ can be generated as

$$q_{d1} = 0.2 + 0.5\cos(\pi t/5), \quad q_{d2} = 0.2 + 0.5\sin(\pi t/5). \tag{37}$$

During the manipulation, the interaction force $f_e = [f_{e1}, f_{e2}]^{\mathrm{T}}$ is considered to be

$$f_{e1} = f_{e2} = \begin{cases} 5, & 0 \leqslant t \leqslant 3, \\ 5 + 2.5(t-3), & 3 \leqslant t \leqslant 5, \\ 10, & 5 \leqslant t \leqslant 10, \\ 10 + 2(t-10), & 10 \leqslant t \leqslant 14, \\ 18 - 3(t-14), & 14 \leqslant t \leqslant 18. \end{cases} \tag{38}$$

The simulations are conducted in two cases with different impedance profiles to illustrate the control effectiveness and show advantages of the proposed impedance controller (Figures 2–6). Case 1: $M_d = I, B_d = 10I, K_d = 21I$; Case 2: $M_d = I, B_d = 10I, K_d = 30I$.

(1) Effectiveness of the proposed CLIC. In the aforementioned two cases, the control parameters for the CLIC are selected as $k_1 = 1, k_2 = 2, \gamma = 2, k_p = 4, \epsilon = 0.01$. From Figures 2 and 5, the proposed CLIC $u = [u_1, u_2]^{\mathrm{T}}$ ensures the convergence of the impedance error $e = [e(1), e(2)]^{\mathrm{T}}$ to a very small neighborhood of zero with a radius of less than 0.002. By comparing between Figures 2 and 3, and between Figures 5 and 6, we can observe that the impedance errors in Figures 2 (Figure 5) converge much faster than those in Figures 3 (Figure 6). This shows the advantages of the robot-environment interaction control term $\beta(e_2, \tau_e)$ in improving transient impedance control performances.

(2) Comparison with the adaptive impedance controllers in [24, 25]. In Case 1, the desired impedance profiles satisfy the factorization in real number field $s^2 I + M_d^{-1} B_d s + M_d^{-1} K_d = s^2 I + 10Is + 21I = (sI + 3I)(sI + 7I)$. Then, the adaptive impedance controllers in [24, 25] can be implemented, where the control gain is selected as 2 and the learning rate of the update law is selected as 4. By comparing the

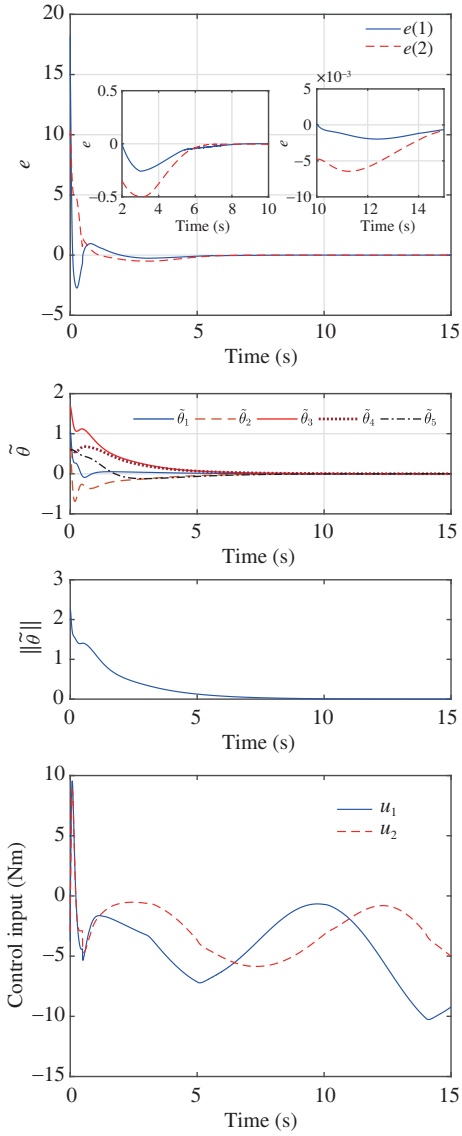

Figure 2 (Color online) Simulation results of the proposed CLIC in Case 1.

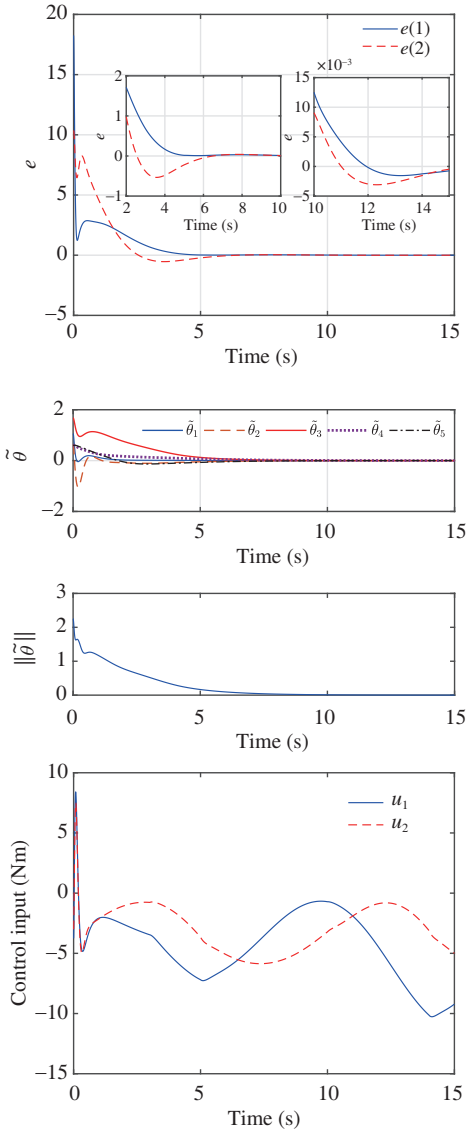

Figure 3 (Color online) The proposed CLIC results in Case 1 without encouragement of the correct robot movements.

control performances between Figures 2 and 4, one can observe that if the desired impedance dynamics can be factorized in real number field, the the proposed CLIC exhibits better transient performance and steady-state performances of impedance error than that exhibited by the adaptive impedance controllers in [24, 25].

In Case 2, the desired impedance dynamics cannot be factorized in real space and the adaptive impedance controllers in [24, 25] cannot be implemented. Based on the proposed CLIC, the good performance of impedance errors in Figure 5 shows the advantages of the proposed CLIC in general applications.

(3) Comparison with the sliding-mode impedance controllers. Based on the passivity-based control theory [32], the sliding-mode impedance controllers were proposed in [19,20], where the switching function can be constructed as $r = [r_1, r_2]^{\mathrm{T}} = \dot{q} - \dot{q}_d + z$ and z is generated as $\dot{z} = Az + K_{pz}(q - q_d) + K_{vz}(\dot{q} - \dot{q}_d) + K_{fz} - \tau_e$ and $K_{pz} = 30I, K_{vz} = 0, K_{fz} = I$. If the sliding mode $\{\dot{r} = 0, r = 0\}$ is reached, then the desired impedance dynamics in (3) can be achieved. The sliding-mode controller in [19] is presented as

$$u = \hat{M}(q)\dot{e}_{eq} + \hat{C}(q, \dot{q})(\dot{q}_d - z) + \hat{F}(\dot{q}) - 5r - \tau_e - [\delta_1 \mathrm{sgn}(r_1), \delta_2 \mathrm{sgn}(r_2)]^{\mathrm{T}}, \tag{39}$$

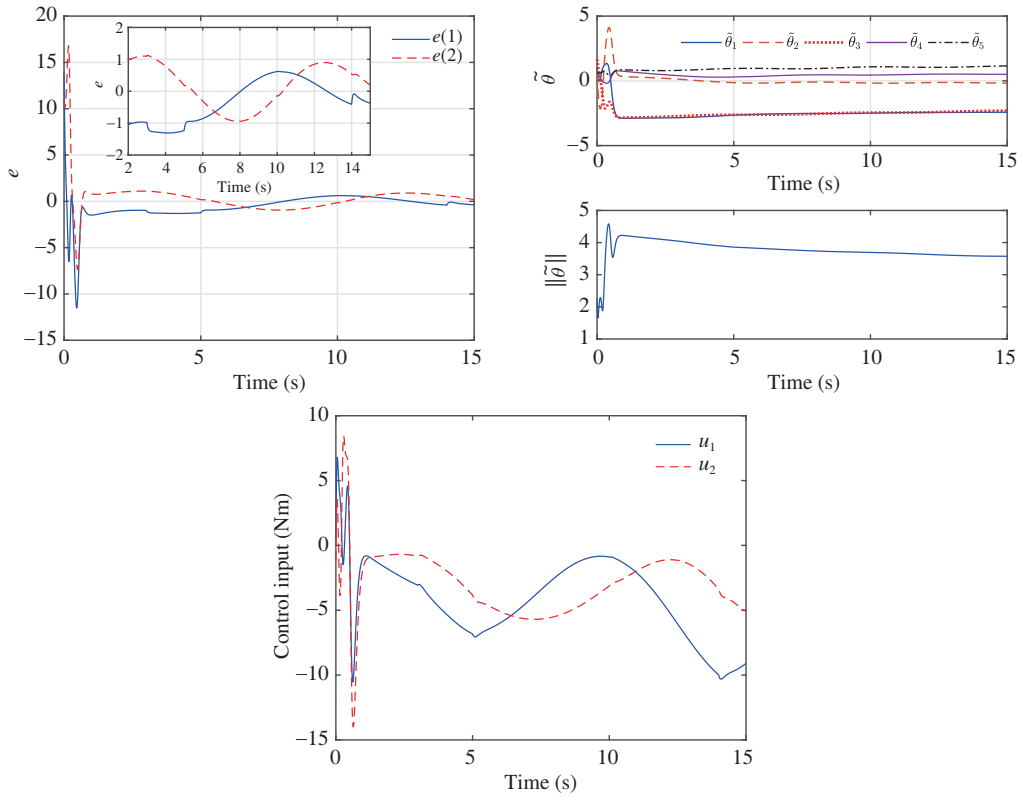

Figure 4 (Color online) Control results of the adaptive impedance controllers [24, 25] in Case 1.

where $\dot{e}_{eq} = \ddot{q}_d - \dot{z}$ and $e_{eq} = \dot{q}_d - z$, the values of estimators $\hat{\theta}_i$ in $\hat{M}(q)$, $\hat{C}(q, \dot{q})$, and $\hat{F}(\dot{q})$ are chosen to be $\hat{\theta}_1 = 0.6, \hat{\theta}_2 = 0.8, \hat{\theta}_3 = 1, \hat{\theta}_4 = \hat{\theta}_5 = 0.4$, and $\delta = [\delta_1, \delta_2]^{\mathrm{T}}$ satisfies $\delta_i > |\tilde{\delta}_i|, i = 1, 2$ with $\tilde{\delta} = [M(q) - \hat{M}]\dot{e}_{eq} + [C(q, \dot{q}) - \hat{C}](\dot{q}_d - z) + [F(\dot{q}) - \hat{F}]$. In theory, the controller in (39) ensures the convergence of r to zero in finite time; subsequently, $r \equiv 0$ ensures that $\dot{r} = 0$. The sliding-mode impedance controller in [20] is given by

$$u = Y(\dot{e}_{eq}, e_{eq}, q, \dot{q})(\hat{\theta} + a) - 5r - \tau_e, \tag{40}$$

where a is a robust term defined as

$$a = \begin{cases} -1.08\dfrac{Y^{\mathrm{T}}r}{||Y^{\mathrm{T}}r||}, & ||Y^{\mathrm{T}}r|| \neq 0, \\ 0, & ||Y^{\mathrm{T}}r|| = 0. \end{cases} \tag{41}$$

To alleviate chattering, the following dead-zone is chosen to replace a in (40):

$$a = \begin{cases} -1.08\dfrac{Y^{\mathrm{T}}r}{||Y^{\mathrm{T}}r||}, & ||Y^{\mathrm{T}}r|| \neq 0.01, \\ -1.08Y^{\mathrm{T}}r/0.01, & ||Y^{\mathrm{T}}r|| \leqslant 0.01. \end{cases} \tag{42}$$

The simulation results of the sliding-mode controllers in (39) and (42) are presented in Figures 7 and 8, respectively. From the two figures, we can see that chattering affects the stability and robustness of sliding-mode controllers. Although the dead-zone implementation alleviates the chattering in [20], chattering still exists in the simulation results. This shows the disadvantages of sliding-mode impedance controllers.

Based on aforementioned analysis, the proposed CLIC using the composite learning law and the robot-environment interaction control term improves the transient and steady-state impedance error performances beyond those of the adaptive impedance controllers in [24, 25] and the sliding-mode impedance

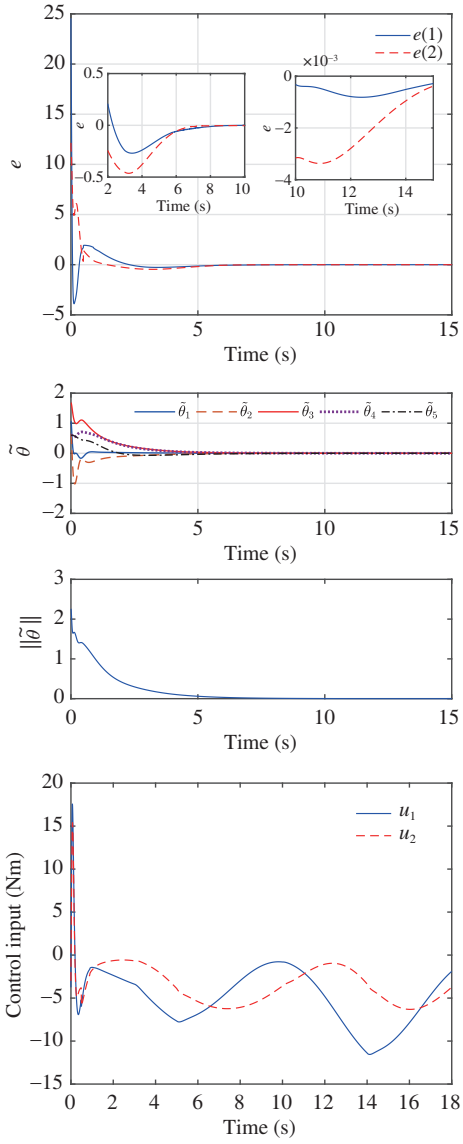

Figure 5 (Color online) The proposed CLIC results in Case 2.

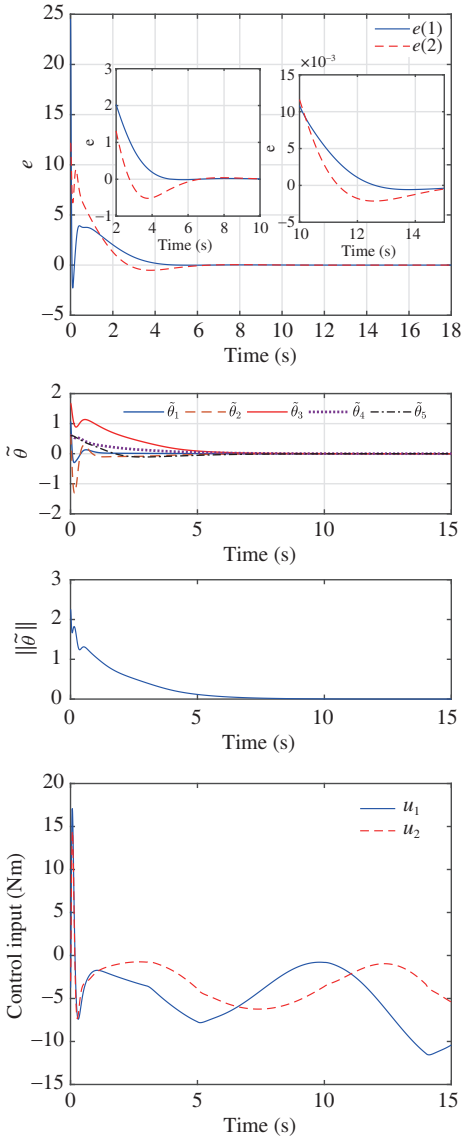

Figure 6 (Color online) The proposed CLIC results in Case 2 without encouragement of the correct robot movements.

controllers in [19,20]. The proposed CLIC shows its advantages in improving impedance control stability and robustness.

5 Conclusion

An impedance controller aims to achieve desired impedance dynamics between the desired-trajectory tracking error and the robot-environment interaction force. The desired impedance dynamics can be achieved if and only if an impedance error converges to zero or its small neighborhoods. Although many impedance controllers have been designed in the past few decades, uncertainty and disturbances in robot modeling continue to severely affect the control stability and robustness.

To improve the impedance control stability and robustness, this study proposes a composite-learning impedance controller for robots with a robot-environment interaction control term to encourage/suppress correct/incorrect robot movements. Convergence of the impedance error is guaranteed by the convergence

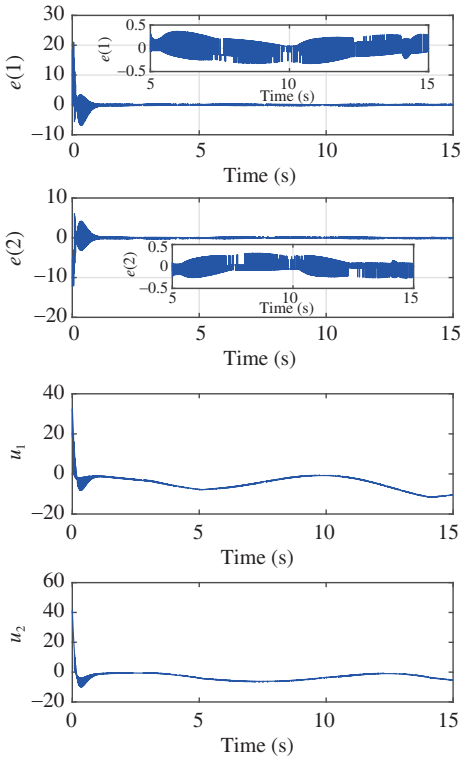

Figure 7 (Color online) Simulation results using the sliding-mode impedance controller in (39) in Case 2.

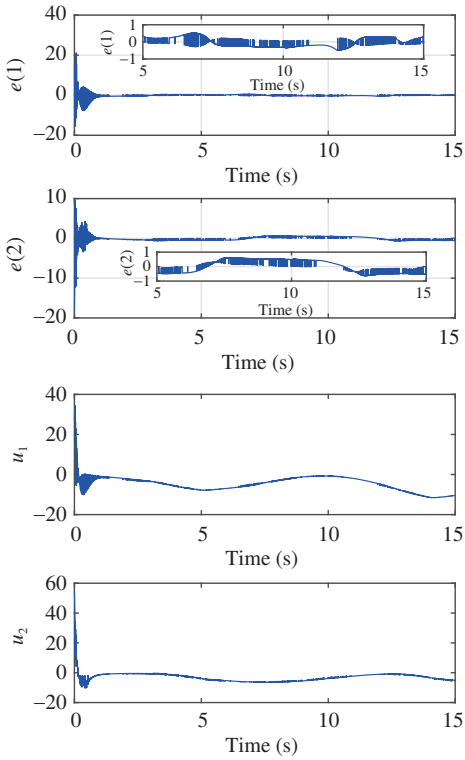

Figure 8 (Color online) Simulation results using the sliding-mode impedance controller in (40) in Case 2.

of the auxiliary error e_2 and the parameter estimation error $\tilde{\theta}$, ensuring that the desired impedance dynamics can be achieved. The simulations on a parallel robot with a five-bar structure illustrate the control effectiveness and advantages in comparison with the existing impedance controllers.

Although variable impedance control is appealing for its ability to realize human-like robot motions, majority of the existing impedance controllers use constant impedance profiles; therefore, it remains an open problem to guarantee the control stability of variable impedance controllers. In the near future, we will design stability-guaranteed variable impedance controllers for robots.

Acknowledgements This work was supported in part by National Natural Science Foundation of China (Grant Nos. 61720106012, 61873268, 61633016), Beijing Natural Science Foundation (Grant No. L182060), Strategic Priority Research Program of Chinese Academy of Sciences (Grant No. XDB32040000), and China Postdoctoral Science Foundation (Grant No. 2019T120405).

References

1 Yu J P, Zhao L, Yu H S, et al. Barrier Lyapunov functions-based command filtered output feedback control for full-state constrained nonlinear systems. Automatica, 2019, 105: 71–79
2 Abdelatti M, Yuan C Z, Zeng W, et al. Cooperative deterministic learning control for a group of homogeneous nonlinear uncertain robot manipulators. Sci China Inf Sci, 2018, 61: 112201
3 He W, Yin Z, Sun C Y. Adaptive neural network control of a marine vessel with constraints using the asymmetric barrier Lyapunov function. IEEE Trans Cybern, 2017, 47: 1641–1651
4 Yu J P, Shi P, Zhao L. Finite-time command filtered backstepping control for a class of nonlinear systems. Automatica, 2018, 92: 173–180
5 Hogan N. Impedance control: an approach to manipulation: Part I-theory. J Dynamic Syst Measurement Control, 1985, 107: 1–7
6 Cui J, Lai M, Chu Z Y, et al. Experiment on impedance adaptation of under-actuated gripper using tactile array under unknown environment. Sci China Inf Sci, 2018, 61: 122202
7 Chu Z Y, Yan S B, Hu J, et al. Impedance identification using tactile sensing and its adaptation for an underactuated gripper manipulation. Int J Control Autom Syst, 2018, 16: 875–886
8 Sun T R, Peng L, Cheng L, et al. Stability-guaranteed variable impedance control of robots based on approximate

dynamic inversion. IEEE Trans Syst Man Cybern Syst, 2019. doi: 10.1109/TSMC.2019.2930582
9 Zhang F, Hou Z G, Cheng L, et al. iLeg—a lower limb rehabilitation robot: a proof of concept. IEEE Trans Human-Mach Syst, 2016, 46: 761–768
10 Saglia J A, Tsagarakis N G, Dai J S, et al. Control strategies for patient-assisted training using the ankle rehabilitation robot (ARBOT). IEEE/ASME Trans Mechatron, 2013, 18: 1799–1808
11 Li Z J, Zhao S, Duan J, et al. Human cooperative wheelchair with brain-machine interaction based on shared control strategy. IEEE/ASME Trans Mechatron, 2017, 22: 185–195
12 Wojtara T, Uchihara M, Murayama H, et al. Human-robot collaboration in precise positioning of a three-dimensional object. Automatica, 2009, 45: 333–342
13 Vukobratovic M, Surdilovic, Ekalo Y, et al. Dynamics and Robust Control of Robot-Environment Interaction. Singapore: World Scientific, 2009
14 Jung S, Hsia T C. Neural network impedance force control of robot manipulator. IEEE Trans Ind Electron, 1998, 45: 451–461
15 Jamwal P K, Hussain S, Ghayesh M H, et al. Impedance control of an intrinsically compliant parallel ankle rehabilitation robot. IEEE Trans Ind Electron, 2016, 63: 3638–3647
16 He W, Dong Y, Sun C Y. Adaptive neural impedance control of a robotic manipulator with input saturation. IEEE Trans Syst Man Cybern Syst, 2016, 46: 334–344
17 Sharifi M, Behzadipour S, Salarieh H, et al. Cooperative modalities in robotic tele-rehabilitation using nonlinear bilateral impedance control. Control Eng Practice, 2017, 67: 52–63
18 Sharifi M, Behzadipour S, Vossoughi G. Nonlinear model reference adaptive impedance control for human-robot interactions. Control Eng Practice, 2014, 32: 9–27
19 Chan S P, Yao B, Gao W B, et al. Robust impedance control of robot manipulators. Int J Robot Autom, 1991, 6: 220–227
20 Mohammadi H, Richter H. Robust tracking/impedance control: application to prosthetics. In: Proceedings of American Control Conference, 2015. 2673–2678
21 Cheah C C, Wang D W. Learning impedance control for robotic manipulators. IEEE Trans Robot Automat, 1998, 14: 452–465
22 Li X, Liu Y H, Yu H Y. Iterative learning impedance control for rehabilitation robots driven by series elastic actuators. Automatica, 2018, 90: 1–7
23 Liang X Q, Zhao H, Li X F, et al. Force tracking impedance control with unknown environment via an iterative learning algorithm. Sci China Inf Sci, 2019, 62: 050215
24 Li Y N, Ge S S. Human-robot collaboration based on motion intention estimation. IEEE/ASME Trans Mechatron, 2014, 19: 1007–1014
25 Li Z J, Huang Z C, He W, et al. Adaptive impedance control for an upper limb robotic exoskeleton using biological signals. IEEE Trans Ind Electron, 2017, 64: 1664–1674
26 Sun T, Peng L, Cheng L, et al. Composite learning enhanced robot impedance control. IEEE Trans Neural Netw Learn Syst, 2020, 31: 1052–1059
27 He W, Dong Y. Adaptive fuzzy neural network control for a constrained robot using impedance learning. IEEE Trans Neural Netw Learn Syst, 2018, 29: 1174–1186
28 Li X, Pan Y P, Chen G, et al. Multi-modal control scheme for rehabilitation robotic exoskeletons. Int J Robot Res, 2017, 36: 759–777
29 Pan Y P, Yu H Y. Composite learning from adaptive dynamic surface control. IEEE Trans Automat Contr, 2016, 61: 2603–2609
30 Pan Y P, Yu H Y. Composite learning robot control with guaranteed parameter convergence. Automatica, 2018, 89: 398–406
31 Wang C, Peng L, Luo L C, et al. Genetic algorithm based dynamics modeling and control of a parallel rehabilitation robot. In: Proceedings of 2018 IEEE Congress on Evolutionary Computation, 2018. 1–7
32 Spong M W, Vidyasagar M. Robot Dynamics and Control. New York: John Wiley & Sons, 2008